

Controlled Alcohol–Ketone Interconversion by Dihydrogen Transfer: An *ab Initio* Study of the Methanol–Formaldehyde Complex

Yisroel Brumer[†] and Moshe Shapiro

Chemical Physics Department, The Weizmann Institute of Science, Rehovot, Israel 76100

Paul Brumer

Chemical Physics Theory Group, Department of Chemistry, University of Toronto, Toronto, Canada M5S 3H6

Kim K. Baldridge*

University of California, San Diego, 9500 Gilman Drive, La Jolla, California 92093-0505

Received: March 12, 2002

An *ab initio* computational study of the reaction pathways for methanol–formaldehyde complexation is presented. This study serves as a prototype for novel dihydrogen exchange between the alcohol and ketone structures, such that the reactants and products are mirror images. The donated hydrogen atoms, both from the alcohol, are the hydroxyl group hydrogen and one of the carbon hydrogen atoms. Whereas the motion of the former hydrogen atom is known to be facile, as facilitated by formation of a hydrogen bond, the barrier to the latter hydrogen atom transfer was not known. In the present work, the barrier for the dihydrogen transfer is determined to be 33.1 kcal/mol, with the reaction proceeding via a hexagonal transition state structure. By contrast, the second excited singlet state is characterized by a potential well at the geometry corresponding to that of the transition state on the ground state surface and manifests the facile donation of both hydrogen atoms. The presence of a sufficiently high ground state surface barrier, coupled with an excited state potential well, is a prerequisite for the coherently controlled interconversion of a chiral alcohol to the analogous ketone and that of the ketone to a chiral alcohol of the *opposite* handedness. Dihydrogen exchange reactions of this type could, therefore, serve as prototypes for coherently controlled racemic purification.

Introduction

The existence of enantiomers is one of the fundamental broken symmetries in nature.^{1–3} It is also one of great practical importance because biological processes are often stereospecific, motivating a long-standing interest in asymmetric synthesis. In recent years we^{4–7} and others^{8–10} have shown that controlled enantioselective dissociation^{4–6} and racemic purification⁷ can be accomplished by optical means, using coherent control techniques.^{6,11,12} Specifically, we have demonstrated that it is possible to use the strong electric dipole–electric field interaction to discriminate between enantiomers and to selectively increase the concentration of a desired enantiomer in a racemic mixture.

For example, in ref 6 we considered the two-photon dissociation of a single quantum state of a B–A–B' molecule to yield BA + B' and B + AB', where B and B' are enantiomers. We demonstrated that coherent control techniques can be used to control the yield of the right-handed (B) vs the left-handed (B') fragment, provided that a specific fragment polarization, i.e., the projection **M** of the total angular momentum along the polarization axis, is selected. Further, in ref 7 we introduced a coherent control scheme for *purifying* a statistical racemic mixture of polarized (**M**-selected) molecules. In this scheme, called “laser distillation”, a racemic mixture was repeatedly excited optically and allowed to relax, using a specific laser

configuration. This approach yields a remarkable degree of enantioselectivity and is controllable by varying a variety of laser parameters. An extension of this scenario to nonpolarized media using three perpendicular lasers has also been developed.¹³ Further, a recent paper¹⁴ provides a general theorem providing conditions under which enantiomeric control with the electric dipole–electric field interaction is possible.

In all scenarios that we have thus far developed^{4–7} the molecule under consideration must be characterized by a chiral ground electronic state and an achiral excited electronic state. Recently,^{4,5} we demonstrated that dimethylallene displays these features and that over 90% enantiomeric excesses can be achieved in **M**-polarized dimethylallene using lasers of reasonable powers. Studies on control in nonpolarized dimethylallene are in progress.

The first step in assessing the utility of a particular molecular system for laser distillation is, therefore, to determine the chiral or achiral characteristics of ground and excited states. The purpose of this paper is to carry out such a study for a novel set of reactions for which the “laser distillation” scheme may be realizable. These reactions involve the synchronous donation of two hydrogens from a chiral alcohol to the analogous ketone through an excited electronic state. As a result, the alcohol becomes the ketone and the ketone becomes an alcohol of either handedness.

Specifically, we previously suggested⁷ that laser distillation could be achieved in this system if the ground state were characterized by a stable complex between the ketone and the

[†] Current address: Department of Chemistry and Chemical Biology, Harvard University, 12 Oxford St., Cambridge, MA, 02139.

chiral alcohol and by an achiral minimum resulting from the synchronous donation of two hydrogens on the excited electronic state. What is particularly intriguing about this scenario is that a small quantity of ketone would serve as a catalyst for converting a racemic mixture of polarized alcohols to the essentially pure enantiomer of choice. We examine the characteristics of the potential surfaces in this paper for a simplified model, demonstrating the desired characteristics. Note that initially we deal, for simplicity, with an achiral alcohol and then provide preliminary results on a chiral alcohol system.

The alcohol plus ketone reaction is an analogue of the more classic metal-catalyzed Meerwein–Ponndorf–Verley (MVP) reduction reaction, which has been studied experimentally since the early 1940s^{15–18} as a method for the reduction of carbonyl compounds. Asymmetric representations of this reduction reaction involving ketones have been widely studied through the use of optically active alcohols as chiral sources, although the potential for high enantioselectivity has not been realized.

The reaction under investigation in this work serves as a prototype for novel dihydrogen exchange between alcohol and ketone structures, such that the reactants and products are mirror images. As an important class of hydrogenation and dehydrogenation reactions, those involving intermolecular concerted dihydrogen transfer have been considered for their obvious mechanistic importance both theoretically and experimentally.^{19–35} Classical examples of such studies include dihydrogen transfer from 1,2-diazene to olefins, acetylenes, and azo compounds,²¹ which have been shown experimentally to have very large driving forces;³⁴ dihydrogen donation to an aromatic system, reactions that also have sizable driving forces^{23,24,29} and dihydrogen transfer from a saturated carbon–carbon linkage to an olefin group^{23,24,32} (dyotropic rearrangements), perhaps the most studied being the ethane–ethylene reaction;^{25,35} Activation energetics for dihydrogen exchange reactions range from essentially thermoneutral to having substantial barriers (>50 kcal/mol), depending on the nature of the species involved. As has been pointed out in several of the previous theoretical studies, the inclusion of electron correlation of sufficient level is critical for accurate estimations of activation energy in these types of reactions.

Our own interest lies in the general characterization of such prototypes for coherently controlled racemic purification. In particular, the detailed reaction profile of the ground and excited states including the understanding of the mechanism and the nature of the kinetic barrier for the methanol–formaldehyde reaction is the focus of the first phase of study. In the consideration of the methanol–formaldehyde reaction, there are several minimum energy structures (Figure 1) and possible mechanisms to consider. These include the reactants [(i) in Figure 1] combining to form a hydrogen-bonded complex (ii), the symmetric exchange of H's through a symmetric transition state (iii), and an uncatalyzed hemi-acetal (iv) reaction. Early theoretical studies of the dihydrogen transfer in the methanol–formaldehyde system were carried out using semiempirical and modest levels of *ab initio* theory.²⁵ McKee et al. considered the enthalpic barrier between the reactant species and symmetric transition state structures, illustrating the serious overestimations provided by semiempirical methods (>50 kcal/mol), as well the importance of electron correlation for prediction of energetics of such a process. The current work expands on the earlier investigations in two ways: the first is a more detailed look at the potential energy surface for this reaction, most importantly including structure (ii) and considerations of excited state surfaces, and second, it includes a more substantial investigation

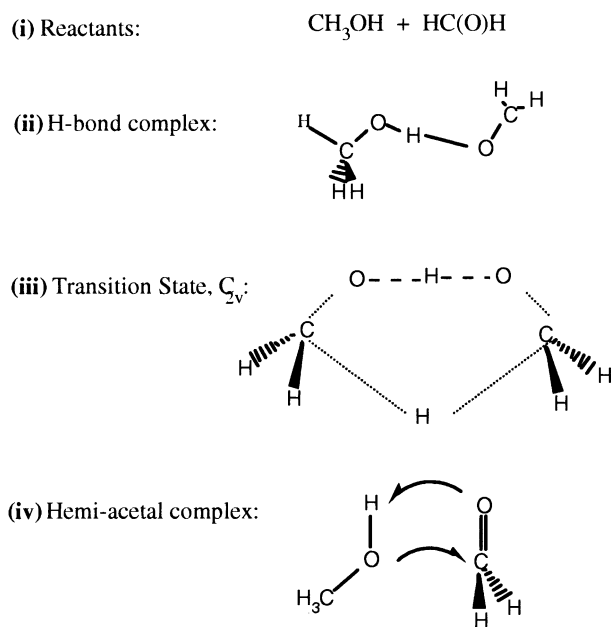


Figure 1. Methanol–formaldehyde complexation structures.

of correlation effects to determine accurate energetics for experimental purposes. Characteristics of the hydrogen-bonded complex are compared to those found in other dihydrogen transfer reactions.

Theoretical Considerations

The molecular structures for the alcohol–ketone system have been determined using a variety of theoretical methods to establish self-consistency in terms of basis sets as well as to explore the effects of dynamic correlation. We report results from restricted Hartree–Fock (RHF), hybrid density functional (HDFT)³⁶ Moller–Plesset perturbation (MP2, MP4),³⁷ and coupled cluster theory with all single and double substitutions augmented by a quasiperturbative accounting of triple excitations (CCSD(T)).³⁸ These calculations were performed using the gradients and search algorithms contained in the GAMESS^{39,40} and GAUSSIAN98⁴¹ programs. In addition, we employed a number of different basis sets to ascertain the effects of basis sets on structure and energetic properties. These include 6-31G-(nd,mp),^{42–45} DZV(2d,p) and DZ(2d,p),⁴⁶ TZV(2d,p),^{47,48} cc-pvdz,⁴⁹ cc-pvtz,⁵⁰ aug-cc-pvdz,⁴⁹ and aug-cc-pvtz,⁵⁰ where $n = 0–2$, $m = 0–1$. The HDFT method employed Becke's three-parameter hybrid exchange functional⁵¹ in combination with the nonlocal correlation provided by the Perdew (1991) expression,⁵² B3PW91.⁵³ We have determined optimal basis set convergence by exploring this large variety of basis sets—investigations that are adequately performed at the RHF level of theory.^{54,55} Subsequently, we have investigated the extent of correlation necessary for prediction. As discussed, the importance of dynamic electron correlation has been illustrated in the literature and is further investigated in this work through the methods laid out above. In addition, careful preliminary study, as well as several other literature investigations,^{25,27,28,35} indicate that the likelihood of needing a multiconfigurational method for this reaction is small. A sufficiently closed-shell representation is determined through preliminary MCSCF computations using the appropriate active space.

Effects of basis set superposition error (BSSE) were investigated using SCF-MI⁵⁶ and found to be negligible. The SCF-MI method is a modification of the Roothaan equations that avoids BSSE in intermolecular interaction calculations, by

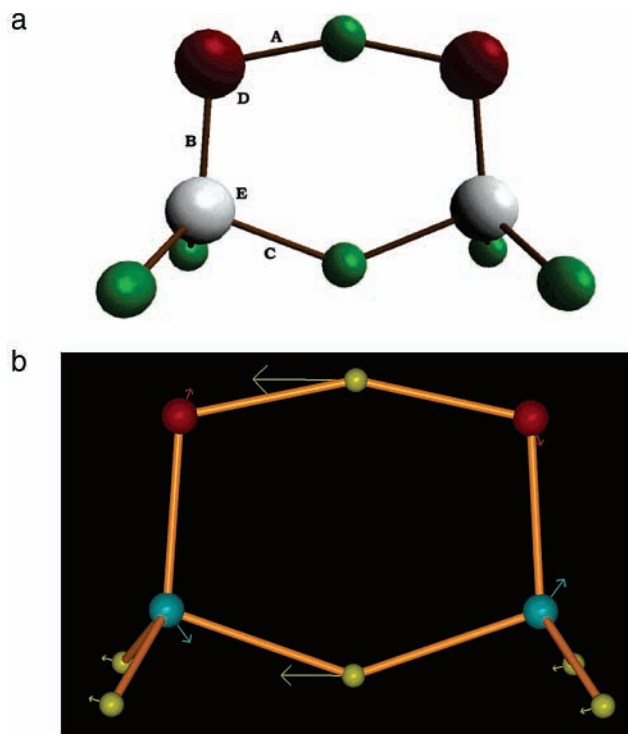


Figure 2. (a) Methanol–formaldehyde transition state. The letters correspond to those in Table 2. Here and below, large gray balls are carbon, small green balls are hydrogen atoms, and large red balls are oxygen atoms. (b) Methanol–formaldehyde transition state with imaginary mode depicted.

expanding the orbitals of each using only its own basis set. The nature of each stationary point was uniquely characterized by analytically calculating and diagonalizing the matrix of energy second derivatives (Hessian) to determine the number of imaginary frequencies and was then depicted using QMView.⁵⁷ Molecular orbital contour plots, used as an aid in the discussion of the results, were generated using the program 3D-PLTORB,⁵⁸ and depicted using QMView.

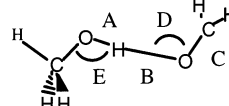
Once the fully characterized transition state structures were located, the intrinsic reaction coordinate (IRC) was followed down to the reactants (note that the path is symmetric about the transition state) using the one-step Euler Method with reaction path stabilization.^{59–62} The IRC is the path of steepest descent in mass-weighted coordinates and provides a convenient definition of the reaction path. Because the gradient at the saddle point is zero, the IRC is initiated by making a small displacement of 10^{-4} hartrees in the direction of the single imaginary normal mode.⁶³

Configuration interaction⁶⁴ computations were performed using the CISD method⁶⁵ together with the DZV(2d,p) basis set, to investigate the first and second excited state surface for the reaction. Specifically, these calculations provided the excited state energies at geometries corresponding to the points along the ground state reaction surface.

Discussion

The degenerate dihydrogen exchange between formaldehyde and methanol is an example of a Woodward and Hoffman⁶⁶ symmetry-allowed reaction. The determination of the transition state of this reaction is simplified under the assumption of C_{2v} symmetry (Figure 2). Other possible transition states were located and found to present high barriers to reaction. Thus, the symmetric path was found to best describe the reaction

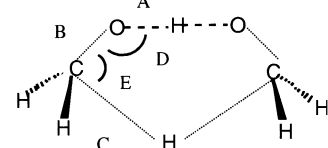
TABLE 1: Geometric Parameters for the Methanol–Formaldehyde H–Bonded Complex at a Variety of Levels of Theory^a



level	A	B	C	D	E
RHF/6-31G(d)	0.949	2.101	1.189	101.2	109.8
RHF/6-31G(2d,p)	0.944	2.114	1.183	101.3	109.7
RHF/DZV(2d,p)	0.944	2.092	1.188	119.2	109.6
RHF/DZ(2d,p)	0.945	2.117	1.189	105.0	109.8
RHF/cc-pVDZ	0.948	2.120	1.186	100.9	109.5
RHF/aug-cc-pVDZ	0.945	2.131	1.188	104.1	110.2
RHF/TZV(2d,p)	0.943	2.137	1.182	104.3	110.1
RHF/cc-pVTZ	0.642	2.168	1.182	102.32	110.4
RHF/aug-cc-pVTZ	0.943	2.136	1.182	104.2	110.5
MP2/cc-pVDZ	0.971	1.983	1.222	97.9	105.8
MP2/DZ(2d,p)	0.969	1.968	1.226	100.6	107.5
MP2/aug-cc-pVDZ	0.972	1.985	1.228	99.2	108.2
MP2/aug-cc-pVTZ	0.968	1.969	1.218	98.8	108.3
B3PW91/DZ(2d,p)	0.970	1.970	1.211	108.5	108.6
B3PW91/aug-cc-pVDZ	0.970	1.974	1.209	108.2	109.0
B3PW91/aug-cc-pVTZ	0.966	1.984	1.202	108.0	109.1

^a Bond lengths are in angstroms; angles are in degrees.

TABLE 2: Geometric Parameters for the Methanol–Formaldehyde Transition State at a Variety of Levels of Theory^a



level	A	B	C	D	E
RHF/6-31G(d)	1.185	1.275	1.355	106.4	106.3
RHF/6-31G(2d,p)	1.178	1.271	1.350	105.6	107.2
RHF/DZV(2d,p)	1.178	1.275	1.343	105.5	107.3
RHF/cc-pVDZ	1.179	1.273	1.351	105.4	107.3
RHF/aug-cc-pVDZ	1.180	1.277	1.346	105.5	107.5
RHF/TZV(2d,p)	1.180	1.272	1.347	105.5	107.4
RHF/cc-pVTZ	1.179	1.270	1.347	105.6	107.4
MP2/cc-pVDZ	1.183	1.297	1.333	105.1	105.8
MP2/DZ(2d,p)	1.185	1.303	1.321	105.9	105.3
MP2/aug-cc-pVDZ	1.194	1.307	1.329	105.6	105.6
MP2/aug-cc-pVTZ	1.188	1.296	1.322	105.6	105.6
B3PW91/DZ(2d,p)	1.184	1.295	1.334	106.0	105.6
B3PW91/aug-cc-pVDZ	1.190	1.295	1.334	106.0	105.8
B3PW91/aug-cc-pVTZ	1.189	1.290	1.333	105.9	105.8

^a Bond lengths are in angstroms; angles are in degrees.

process. That this optimal geometry (Table 2) is indeed a saddle point on the molecular hypersurface was verified by diagonalizing the mass-weighted Hessian matrix, giving all normal modes and corresponding frequencies. This yielded one negative force constant, as is characteristic of a transition state. The corresponding imaginary frequency is found to be approximately -1500 cm^{-1} (variations from -1360 to -1530 cm^{-1} across the most accurate HDFT and MP2 methodologies), indicating a rather sharply curved energy surface in the direction of the reaction coordinate. This imaginary mode is of B_2 symmetry, which consists of the set of atomic displacements displayed in Figure 2b. One can clearly see that the primary motion is one of the symmetric hydrogens to form methanol, demonstrating the concerted exchange of both hydrogens.

Structurally, the CO bonds of the transition state complex are intermediate in length (1.290 \AA) between formaldehyde

(1.198 Å) and methanol (1.416 Å). The four central H bonds are quite long (1.189 and 1.333 Å), and the peripheral CH bonds remain at 1.099 Å. The peripheral hydrogens are bent back, again being intermediate between formaldehyde and methanol.

The primary goal of the calculations is to achieve a degree of accuracy of structural surface characteristics and associated energetics that will be chemically meaningful to guide future experimental studies. An acceptable level of basis set adequacy is given by structural invariance with increasing basis set size at conventional closed shell Hartree–Fock levels, subsequently supplemented by dynamic correlation, in this case, to access the most accurate energetic information. We have employed a large number of basis sets to identify structural convergence for all features of the surface studied in this work and determined that no less than the double- ζ plus polarization level provides the overall best accuracy for our purposes. Given that, the effects of basis set on the particular geometry of the transition state are very small, although the C–O and C–H bond lengths do change by ~ 2 pm and the O–H bond distance by ~ 1 pm when correlation is added. The values of the angles are not noticeably affected.

Additionally, the need for multiconfigurational SCF (MC-SCF)⁶⁷ treatments, particularly for the transition state structure, needs to be considered. Such considerations have been made on analogous dihydrogen exchange reactions and found to be unnecessary. As well, preliminary MCSCF calculations with the appropriate active space reveal coefficients of the SCF configuration in the MCSCF expansion that indicate that the transition state structure is well represented by the SCF configuration, and therefore dynamic correlation treatments, which in this work have been investigated using a variety of methods, will be adequate.

Following the single imaginary mode of the transition state enables a broader investigation of the reaction process, giving the intrinsic reaction coordinate (IRC) path, which we have computed at both uncorrelated (RHF) and correlated (MP2 and HDFT) levels of theory. The effects of basis set choice on the qualitative features of the reaction process are modest. However, inclusion of dynamic correlation greatly influences the energetic features, depending on the particular method of choice.

The search for stationary points from the point of the transition state complex and along the IRC yields the two highly stable reactant structures, methanol (CH₃OH) and formaldehyde (CH₂O), at large intermolecular distances, i.e., the “bimolecular state”. In addition one finds along the reaction path (even at the RHF/6-31G(d) level) a structure resembling a weak Van der Waals complex, with one imaginary mode, which, when followed, leads to a hydrogen-bonded complex less than 0.5 kcal/mol lower in energy and with slightly shorter internuclear distances (Figure 3). This hydrogen-bonded structure is indeed a stable structure, as characterized by calculating the Hessian, which is positive and definite, and is believed to be the overall minimum energy structure considered (Figure 4). Although an exhaustive search of the potential energy hypersurface is not feasible, a number of investigations were carried out to confirm that no other minima exist in the vicinity.

Table 1 summarizes the structural information for the hydrogen-bonded complex at a variety of levels of theory. Although the bimolecular state does not display great sensitivity to the choice of basis set or to the inclusion of electron correlation, the H-bonded structure clearly does, as evident from the Table 1 parameters. It is of interest to note that, though the OH bond length shows modest variation with inclusion of dynamic correlation (calculated ~ 2.5 pm), the hydrogen bond,

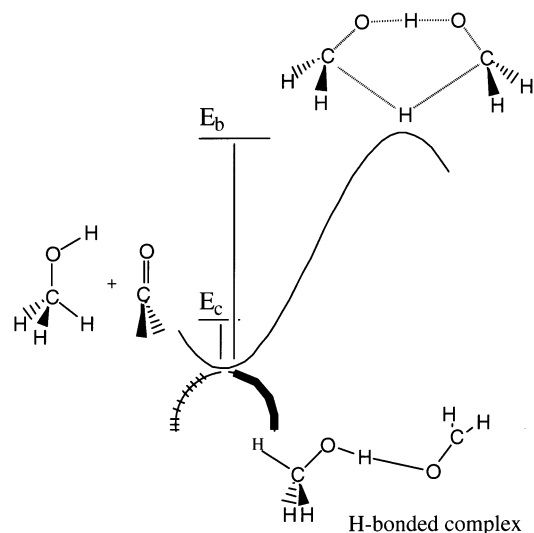


Figure 3. Reaction profile schematic for the methanol–formaldehyde complexation process. The IRC from the transition state leads directly to the van der Waals complex, as discussed in the text. Further elongation of the inter-carbon distance leads to the bimolecular state. Alternatively, following the negative eigenvalue of the van der Waals complex leads to the hydrogen-bonded structure.

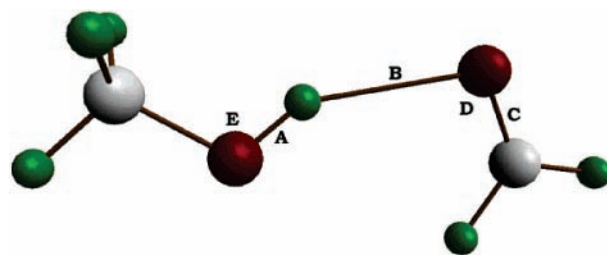


Figure 4. Hydrogen-bonded methanol–formaldehyde complex. The letters correspond to those in Table 1.

B, is very sensitive, changing as much as 15 pm. In addition, the bond angles, particularly the COH value, are sensitive to the inclusion of correlation, increasing by $\sim 4^\circ$.

In general, hydrogen bond complexes span a large range of strengths (1–40 kcal/mol), dependent on the net charge and polarity of the accepting lone pair involved in the particular complex. Clearly, the stability of such a complex for dihydrogen exchange reactions varies according to donors and acceptors that affect the balance of intermolecular energy and internal energy for the complex. Structurally, in this case, we see a relatively weak hydrogen bond complex; that is, a lengthening of the O–H–O distance and a lengthening of the donating OH bond, as compared to a totally symmetric transition state structure (1.185 to 1.913 Å and 1.185 to 1.983 Å, respectively).

As mentioned, the energetic features of the reaction process are greatly influenced by the inclusion of dynamic correlation. We have computed both the energy difference between the hydrogen-bonded complex and reactants and the energy difference between the hydrogen-bonded complex and the transition state (Table 3). To access the most accurate values for these parameters, we have investigated a variety of basis sets as well as methods of dynamic correlation. The most extensive basis set investigations were performed at the RHF level, which can be used as a gauge of basis set limits. This was then followed by MP2, MP4, HDFT, and CCSD(T) computations as well as select single point computations at what was determined to be the optimal basis set for the species involved, aug-cc-pVTZ.

TABLE 3: Activation Energy and H-Bonded Complexation Energy (Including ZPE) for the Reaction Process Shown in Figure 3 at Several Levels of Theory (kcal/mol)

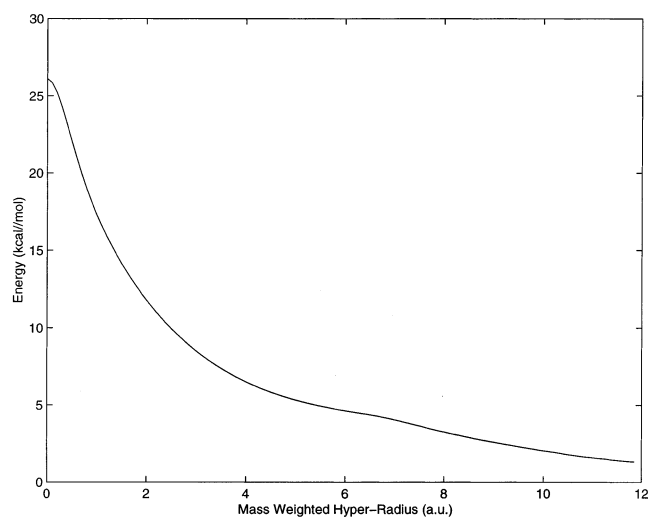
basis set	ΔE_1^a	ΔE_2^b
RHF/6-31G(d)	57.4	3.73
RHF/6-31G(2d,p)	55.8	3.60
RHF/DZV(2d,p)	55.0	3.01
RHF/DZ(2d,p)	52.0	2.86
RHF/cc-pVDZ	55.3	3.91
RHF/aug-cc-pVDZ	54.8	2.64
RHF/TZV(2d,p)	56.0	2.92
RHF/cc-pVTZ	55.5	2.66
RHF/aug-cc-pVTZ	55.3	2.20
MP2/cc-pVDZ	32.6	6.23
MP2/DZ(2d,p)	31.4	4.64
MP2/aug-cc-pVDZ	31.1	4.32
MP2/aug-cc-pVTZ	29.5	4.18
MP4(SDQ)/cc-pVDZ//A*	37.1	4.47
MP4(SDQ)/cc-pVDZ//B*	39.8	4.57
MP4(SDQ)/aug-cc-pVDZ//A*	36.1	3.74
MP4(SDQ)/aug-cc-pVDZ//B*	36.4	3.88
MP4(SDQ)/cc-pVDZ	37.7	4.10
MP4(SDQ)/aug-cc-pVDZ	36.6	3.51
B3PW91/DZ(2d,p)	18.8	3.13
B3PW91/aug-cc-pVDZ	22.3	2.48
B3PW91/aug-cc-pVTZ	23.4	2.08
CCSD(T)/cc-pVDZ//A ^c	(38.0) ^d 33.8	(4.44) 4.68
CCSD(T)/cc-pVDZ//B ^c	(38.4) 34.3	(4.74) 5.09
CCSD(T)/aug-cc-pVDZ//A ^c	(37.2) 32.6	(3.73) 4.09
CCSD(T)/aug-cc-pVDZ//B ^c	(37.5) 33.1	(3.86) 4.29
CCSD(T)/cc-pVDZ	34.6	4.24
CCSD(T)/aug-cc-pVDZ	33.2	3.62

^a $\Delta E_1 = E(\text{TS}) - E(\text{H-bond complex})$. ^b $\Delta E_2 = E(\text{reactants}) - E(\text{H-bond complex})$. ^c Single point energy calculated at either geometry A = B3PW91/aug-cc-pVTZ or B = MP2/aug-cc-pVTZ. ^d Value in parentheses is without triples contribution.

At the highest level of theory considered, CCSD(T) predicts a complexation energy of 3.62 kcal/mol and an activation energy of 33.2 kcal/mol. One sees fairly dramatic differences across RHF, MP2, MP4, and CCSD(T), as is best demonstrated by comparisons across parallel basis sets for the three methods. In any of these comparisons, one sees that the RHF predictions for ΔE_1 are about twice those of MP2 and two and a half times those of HDFT. In the case of ΔE_2 values, the range is much smaller and so the differences among methods less obvious, but still significant. At any of the highest levels of theory considered, the reactants and the H-bonded complex all lie within a 4 kcal/mol range.

As has been noted, for comparisons of energy differences calculated by MP2 vs HDFT, MP2 typically overshoots the “true” barrier by some degree, whereas HDFT underestimates the “true” barrier. Here one sees that HDFT results are in fact quite low for this reaction process. Several single point energy computations were performed using both the B3PW91/aug-cc-pVTZ and MP2/aug-cc-pVTZ optimized geometries, which were determined to be optimally converged basis sets for this reaction process. As the structural predictions were very close with these two basis sets, the respective energetic comparisons show also very similar results, being well within a 0.5 kcal/mol range, and additionally bring the HDFT energetic predictions back into a better agreement with all the other data. The utility of HDFT for accurate geometries followed by single point energy computations performed with more traditional dynamic correlation treatments has been previously noted by one of us in the literature.

The most extensive correlative treatments, MP4 and CCSD(T), were carried out for more accurate determination of energetic predictions, as well as a better convergence of

**Figure 5.** Plot of energy vs reaction coordinate for the methanol–formaldehyde complexation process at the B3PW91/aug-cc-pVDZ level.

numbers. Overall, the data show that inclusion of dynamic correlation such as MP2 decreases (increases) ΔE_1 (ΔE_2), whereas more extensive correlative treatments, either via MP4 or CCSD(T), then again increase (decrease) ΔE_1 (ΔE_2) over MP2 values. It is interesting to note that the contributions of a triple over a double split in the valence set provides over 1 kcal lowering of energy at the correlated levels, and yet no difference at the RHF level, and the additional augmentation of either the double or triple split provides nearly a full kilocalorie lowering of energy. One can see the large contribution of the triples substitution by the comparison of the CCSD vs CCSD(T) data, which is on the order of 4 kcal/mol. This is also clear if one compares the MP4(SDQ) numbers, which are missing the triples contribution, which are on par with the CCSD numbers, again both without the contribution of triples substitutions in the dynamic estimates.

As mentioned, the qualitative comparison of the IRC among the various methods (RHF, MP2, and B3PW91) confirmed that all of the major structural features along the path were as those predicted by the RHF level of theory. A plot of energy versus reaction coordinate at the B3PW91/aug-cc-pVDZ computational level is given as a representative illustration in Figure 5.

Having characterized the reaction processes, molecular orbital analyses (Figure 6) enabled further elucidation of the reaction mechanism. The present reaction bears definite similarities to the classic ethane–ethylene reaction investigated by Feller et al.,³⁵ implying that nondynamical correlation will have little effect on the properties of the alcohol–ketone system. Nevertheless, fully optimized reaction space methodologies could potentially provide further insight into the electronic rearrangements that occur during the reaction. Regardless, as the first step to such an orbital analysis, and to identify clearly the essential changes along the reaction path, we have generated both conventional MOs as well as MOs that are localized inside and outside the reaction zone.

In the σ frame of this activated complex one can identify a series of six cyclic MOs as arising from 1s orbital contributions of the hydrogens and sp^3 -mixed orbitals from the heavy atoms, carbon and oxygen. The energetic ordering of these cyclic MOs is analogous to the classical benzene Huckel orbitals with 0, 1, 2, and 3 nodes. In particular, HOMO-8, HOMO-2, and HOMO-3 (Figure 6a–c) represent the filled members of this set and LUMO, LUMO+1, and LUMO+6 (Figure 6d–f) are the

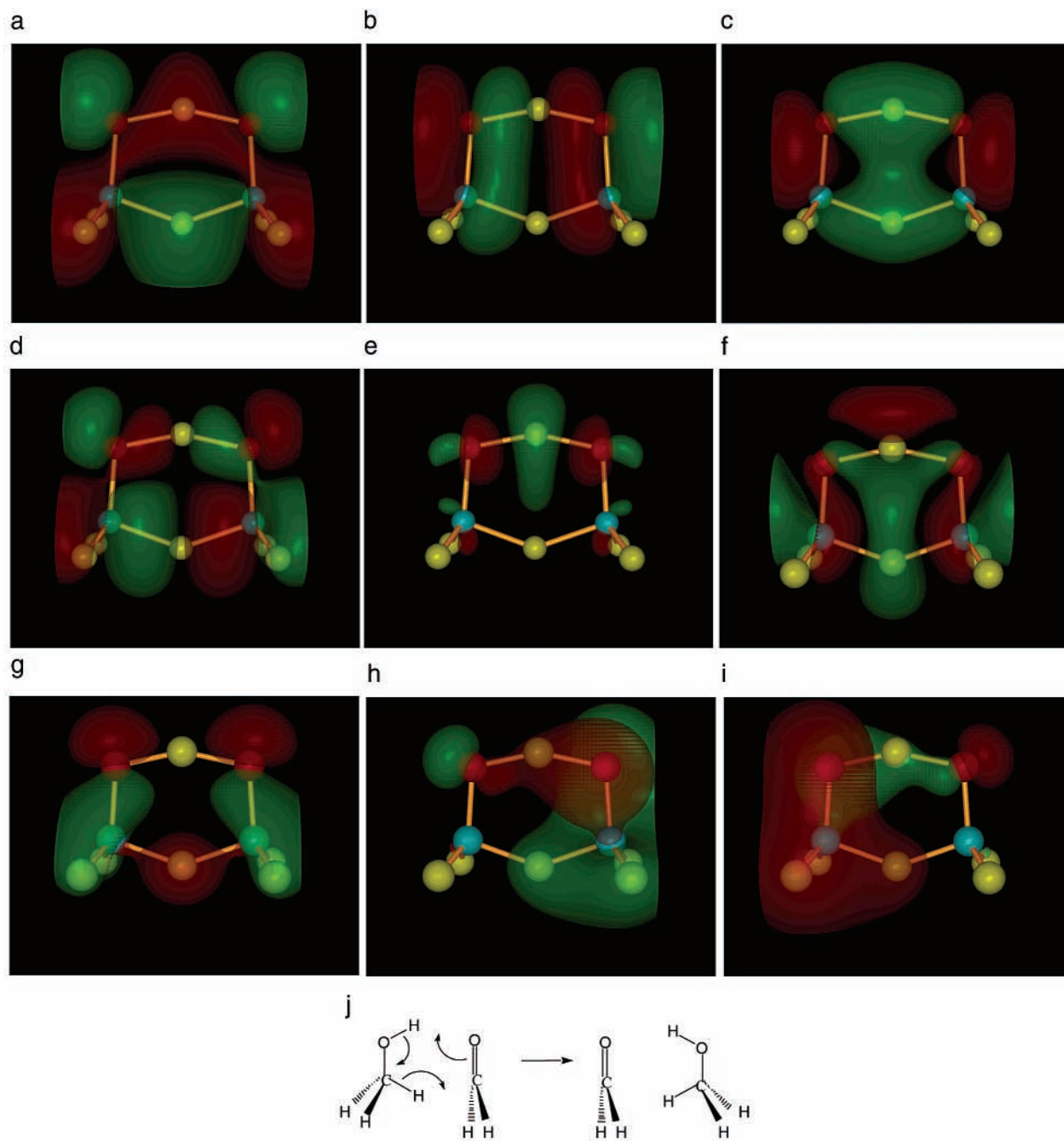


Figure 6. Contour plots of molecular orbitals (as designated) of the methanol–formaldehyde B3PW91/aug-cc-pVDZ transition state structure. The plots were generated using the program 3D-PLTORB and depicted using QMView, with contour values of approximately 0.02 au for both phases. The positive phase is green, the negative phase is red. (a) HOMO-2. (b) HOMO-3. (c) HOMO-8. (d) LUMO. (e) LUMO+1. (f) LUMO+6. (g)–(i) Localized MOs of the activated complex. (j) Schematic diagram of orbital deformation corresponding to the intermediate stages illustrated in Figure 6e–g.

virtuals. Unlike the ethane–ethane system in which the high symmetry of the activated complex (D_{2h}) leads to symmetry-required degeneracies and well-defined nodal planes, the lower symmetry of the methanol–formaldehyde system splits that degeneracy and results in less well-defined nodal planes. The highest of these in-plane σ orbitals (HOMO-2) displays a node perpendicular to the principal C_2 axis of the molecule and resembles two π^* orbitals in symmetric combination bridged by the 1s of the hydrogens. The next highest of these (HOMO-3) in-plane σ orbitals has a clear node along one of the geometric mirror planes of the molecule that passes through the hydrogens; this contribution most closely resembles CO π orbitals in antisymmetric combination. The lowest in this set of σ orbitals

(HOMO-8) can be viewed as a fully symmetrical set of π orbitals bridged by hydrogens.

An alternative SCF MO interpretation of the transition state can be obtained by generating molecular orbitals that are localized inside and outside the reaction zone. This can be done by following the Edmiston–Ruendberg localization procedure.⁶⁸ When this is done, one obtains a slightly different look at the reaction zone (Figure 6g–i). The SCF wave function formed with the MOs of Figure 6e–g can be thought of as representing the intermediate stage of the continuous and concerted orbital shifts and deformations from the reactants to the products, summarized by the schematic diagram of Figure 6j. Each of the activated complex depictions is localized into a

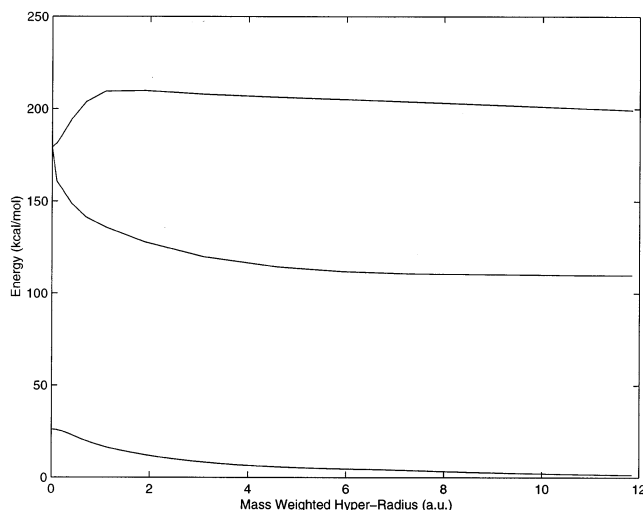


Figure 7. Energy as a function of the reaction coordinate for the same process and level of theory as in Figure 5. The lowest curve is the ground electronic state; the two upper curves are the first two excited states.

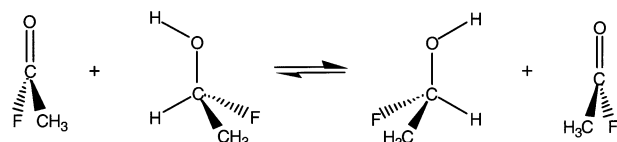


Figure 8. Schematic of substituted dihydrogen transfer system.

three-center bond covering three adjacent atoms (e.g., 6e, OHO, 6f, HCO, 6g, OCH).

Having completed the characterization of the ground state we consider the results of configuration interaction computations used to probe the excited state surfaces for this process. Specifically, the behavior of the excited state surfaces was studied along the geometries of the ground state minimum energy path at the CISD/aug-cc-pVDZ level of theory. Although the first excited state surface shows features not unlike those of the ground state, the second excited state surface displays some interesting properties (Figure 7). In particular, the minimum energy structure along the IRC exists at the ground state surface saddle point, with higher energy structures at the geometries of the ground state reactants and van der Waals complex. Thus, even at this relatively modest level of theory, we note the required structure for coherent control via laser distillation,⁷ i.e., the existence of minima in the excited state at the geometry of the ground state maximum along the reaction path.

The system explored above lacks one feature central to the laser control. That is, the alcohol in the above computation is achiral. For this reason we began a study of the effects of substitution on the prototype reaction. In particular, we considered dihydrogen transfer from 1-fluoro-1-methylformaldehyde to 1-fluoro-1-methylmethanol (Figure 8), a system that allowed us to observe the effects of substitution and chirality, without breaking the reactant–product symmetry. In this case the products do not have to have the same stereochemistry as the reactants and can thus lead to racemization.

One interesting effect of substitution is the possible existence of two transition states: one with C_2 symmetry (with the methyl groups cis to one another) and one of C_s symmetry (with the methyl groups trans to one another). The latter, lower energy configuration, is shown in Figure 9. The C_2 transition state was found to be very similar to that of the unsubstituted system,

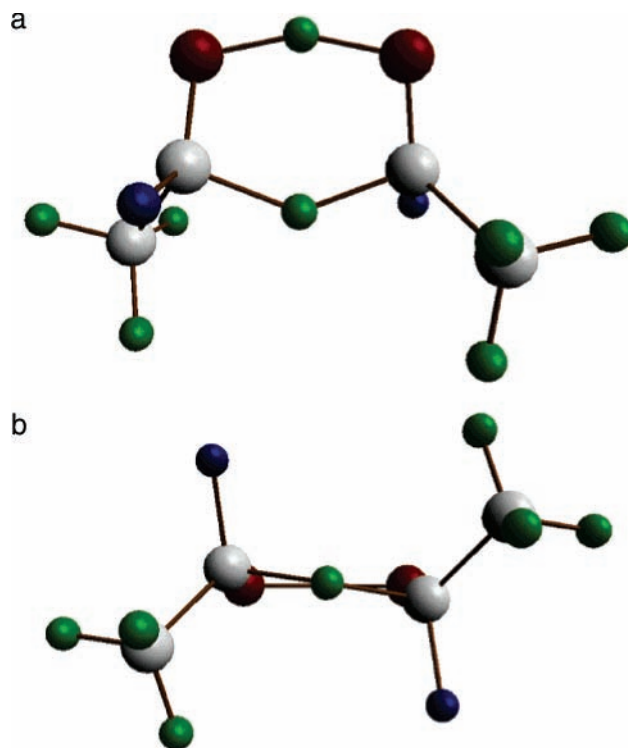


Figure 9. (a) C_2 transition state structure for the dihydrogen transfer from 1-fluoro-1-methylmethanol to 1-fluoro-1-methylformaldehyde. Atom identity is as above, with the addition that intermediate size dark balls denote fluorine atoms. (b) “Bottom” view of the complex shown in part (a). Here the twist that reduces steric hindrance and breaks the C_{2v} symmetry is evident.

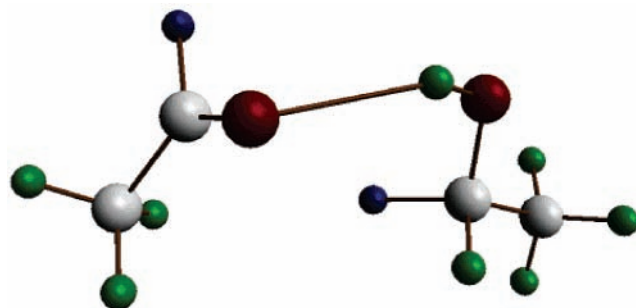


Figure 10. H-bonded complex for the dihydrogen transfer from 1-fluoro-1-methylmethanol to 1-fluoro-1-methylformaldehyde.

except that it displayed an additional twist that reduces steric hindrance. The minimum energy structure (Figure 10) in this reaction process was found to be similar to the methanol–formaldehyde complexation reaction but differs from the analogous unsubstituted complex by a dihedral twist, which again serves to reduce steric interactions.

This considerable change in the geometry of the global minimum is significant for coherent control because it increases the possible overlap between the minimum energy structure on the ground state surface and the structure on the excited state surface corresponding to the ground state transition state geometry. This should significantly enhance the Franck–Condon factors for excitation from the ground to excited state, providing a coherent control enabled process that is much more feasible, and much more interesting, than the unsubstituted reaction. These results also motivated additional studies of alternative substituents to further enhance the wave function overlap.

Conclusions

We have investigated the methanol–formaldehyde dihydrogen donation reaction process in the ground electronic state to a high degree of accuracy. The general features of the excited states along this path have also been investigated. Our computations have elucidated the transition state geometry, the barrier height, the hydrogen bond complexation energy, and the general mechanism of this reaction. They have verified the fundamental requirement for coherent control of asymmetric synthesis, i.e., the nature and relative positioning of the minima in the ground and excited states. Further studies, designed to assess the range of control for these systems, are in progress.

Acknowledgment. This work was supported by a grant from the U.S. Office of Naval Research. K.K.B. thanks the Fulbright Foundation for support during the first part of this research, and NSF-DBI-0078296 for more recent efforts.

References and Notes

- Barron, L. D. *Molecular Light Scattering and Optical Activity*; Cambridge University: Cambridge, U.K., 1982.
- Barron, L. D. *Chem. Soc. Rev.* **1986**, *15*, 189.
- Woolley, R. G. *Adv. Phys.* **1976**, *25*, 27–52.
- Derety, E.; Shapiro, M.; Brumer, P. *J. Phys. Chem. A* **2001**, *105*, 9509.
- Gerbasi, D.; Shapiro, M.; Brumer, P. *J. Chem. Phys.* **2001**, *115*, 5349.
- Shapiro, M.; Brumer, P. *J. Chem. Phys.* **1991**, *95*, 8658.
- Shapiro, M.; Frishman, E.; Brumer, P. *Phys. Rev. Lett.* **2000**, *84*, 1669.
- Fujimura, Y.; Gonzalez, L.; Hoki, K.; Kroener, K.; Manz, J.; Ohtsuki, Y. *Angew. Chem., Int. Ed. Engl.* **2000**, *39*, 4586.
- Hoki, H.; Ohtsuki, Y.; Fujimura, Y. *J. Chem. Phys.* **2001**, *114*, 1575.
- Hoki, K.; Kroener, D.; Manz, J. *Chem. Phys.* **2001**, *267*, 59.
- Rice, S. A.; Zhao, M. *Optical Control of Molecular Dynamics*; Wiley: New York, 2000.
- Shapiro, M.; Brumer, P. *Adv. Atom. Mol. Opt. Phys.* **2000**, *42*, 287.
- Shapiro, M.; Frishman, E.; Brumer, P. Manuscript in preparation.
- Gerbasi, D.; Shapiro, M.; Brumer, P. Manuscript in preparation.
- Brumer, P.; Frishman, E.; Shapiro, M. *Phys. Rev. A* **2002**, *6501*, U682–U684.
- Akamanchi, K. G.; Noorani, V. R. *Tetrahedron Lett.* **1995**, *36*, 3571–3572.
- Degrauw, D. F.; Peters, J. A.; Vanbekkum, H.; Huskens, J. *Synthesis-Stuttgart* **1994**, 1007–1017.
- Fujita, M.; Takarada, Y.; Sugimura, T.; Tai, A. *Chem. Commun.* **1997**, 1631–1632.
- Nishide, K.; Shigetani, Y.; Obata, K.; Node, M. *J. Am. Chem. Soc.* **1996**, *118*, 13103–13104.
- Agrafiotis, D. K.; Rzepa, H. S. *J. Chem. Soc., Chem. Commun.* **1987**, 902–904.
- Agrafiotis, D. K.; Rzepa, H. S. *J. Chem. Soc., Perkin Trans. 2* **1989**, 475–488.
- Back, R. A. *Rev. Chem. Intermed.* **1984**, *5*, 5293–5323.
- Flood, E.; Skancke, P. N. *Chem. Phys. Lett.* **1978**, *54*, 53–56.
- Hagenbuch, J.-P.; Stampfli, B.; Vogel, P. *J. Am. Chem. Soc.* **1981**, *103*, 284–291.
- Mackenzie, K.; Proctor, G.; Woodnutt, D. J. *Tetrahedron* **1987**, *43*, 5981–5993.
- McKee, M. L.; Shevlin, P. B.; Rzepa, H. S. *J. Am. Chem. Soc.* **1986**, *108*, 5793–5798.
- McKee, M. L. *Chem. Phys. Lett.* **1990**, *165*, 265–271.
- McKee, M. L.; Squillacote, M. E.; Stanbury, D. M. *J. Phys. Chem.* **1992**, *96*, 3266–3272.
- McKee, M. L.; Stancury, D. M. *J. Am. Chem. Soc.* **1992**, *114*, 3214–3219.
- Paquette, L. A.; Kesselmayer, M. A.; Rogers, R. D. *J. Am. Chem. Soc.* **1990**, *112*, 284–291.
- Pasto, D. J.; Chipman, D. M. *J. Am. Chem. Soc.* **1979**, *101*, 2290–2296.
- Pasto, D. J. *J. Am. Chem. Soc.* **1979**, *101*, 6852–6857.
- Reetz, M. T. *Tetrahedron* **1973**, *29*, 2189–2194.
- Skancke, P. N. *Chem. Phys. Lett.* **1977**, *47*, 259–264.
- Stanbury, D. M. *Inorg. Chem.* **1991**, *30*, 1293–1296.
- Feller, D. F.; Schmidt, M. W.; Ruedenberg, K. *J. Am. Chem. Soc.* **1982**, *104*, 960.
- Parr, R. G.; Yang, W. *Density Functional Theory of Atoms and Molecules*; Oxford University Press: New York, 1989.
- Møller, C.; Plesset, M. S. *Phys. Rev.* **1934**, *46*, 618–622.
- Raghavachari, K.; Trucks, G. W.; Pople, J. A.; Head-Gordon, M. *Chem. Phys. Lett.* **1989**, *157*, 479.
- Schmidt, M. W.; Baldrige, K. K.; Boatz, J. A.; Elbert, S. T.; Gordon, M. S.; Jensen, J. H.; Koseki, S.; Matsunaga, N.; Nguyen, K. A.; Su, S.; Windus, T. L.; Elbert, S. T. *J. Comput. Chem.* **1993**, *14*, 1347.
- Schmidt, M. W.; Baldrige, K. K.; Boatz, J. A.; Jensen, J. H.; Koseki, S.; Gordon, M. S.; Nguyen, K. A.; Windus, T. L.; Albert, S. T. *QCPE* **1990**, *10*.
- Frisch, M. J.; Trucks, G. W.; Schlegel, H. B.; Scuseria, G. E.; Robb, M. A.; Cheeseman, J. R.; Zakrzewski, V. G.; Montgomery, J. A.; Stratmann, R. E.; Burant, J. C.; Dapprich, S.; Millam, J. M.; Daniels, A. D.; Kudin, K. N.; Strain, M. C.; Farkas, O.; Tomasi, J.; Barone, V.; Cossi, M.; Cammi, R.; Mennucci, B.; Pomelli, C.; Adamo, C.; Clifford, S.; Ochterski, J.; Petersson, G. A.; Ayala, P. Y.; Cui, Q.; Morokuma, K.; Malick, D. K.; Rabuck, A. D.; Raghavachari, K.; Foresman, J. B.; Cioslowski, J.; Ortiz, J. V.; Stefanov, B. B.; Liu, G.; Liashenko, A.; Piskorz, P.; Komaromi, I.; Gomperts, R.; Martin, R. L.; Fox, D. J.; Keith, T.; Al-Laham, M. A.; Peng, C. Y.; Nanayakkara, M. W.; Gonzalez, C.; Challocombe, M.; Gill, P. M. W.; Johnson, B. G.; Chen, W.; Wong, M. W.; Andres, J. L.; Head-Gordon, M.; Replogle, E. S.; Pople, J. A. *Gaussian98-DFT*, revision A.1; Gaussian, Inc.: Pittsburgh, PA, 1998.
- Binning, R. C., Jr.; Curtiss, L. A. *J. Comput. Chem.* **1990**, *11*, 1206–1216.
- Ditchfield, R.; Hehre, W. J.; Pople, J. A. *J. Chem. Phys.* **1971**, *54*, 724–728.
- Hariharan, P. C.; Pople, J. A. *Theor. Chim. Acta* **1973**, *28*, 213.
- Hehre, W. J.; Ditchfield, R.; Pople, J. A. *J. Chem. Phys.* **1972**, *56*, 2257.
- Dunning, T.; Hay, P. Gaussian basis sets for molecular calculations. In *Modern theoretical chemistry*; Schaefer, H. F., Ed.; Plenum Press: New York, London, 1977; p 1.
- Dunning, T. H. *J. Chem. Phys.* **1971**, *55*, 716–723.
- Dunning, T. H. *J. Chem. Phys.* **1971**, *55*, 3958–3966.
- Woon, D. E.; Dunning, T. H. *J. Chem. Phys.* **1993**, *98*, 1358.
- Kendall, R. A.; Dunning, T. H.; Harrison, R. J. *J. Chem. Phys.* **1992**, *96*, 6796.
- Perdew, J. P.; Wang, Y. *Phys. Rev. B* **1992**, *45*, 13244.
- Perdew, J. P.; Burke, K.; Wang, Y. *Phys. Rev. B* **1996**, *54*, 16533–16539.
- Perdew, J. P.; Chevary, J. A.; Vosko, S. H.; Jackson, K. A.; Pederson, M. R.; Singh, D. J.; Fiolhais, C. *Phys. Rev. B* **1992**, *46*, 6671–6687.
- Taylor, P. R. *Int. J. Quantum Chem.* **1991**, *39*, 227–228.
- Taylor, P. R. Accurate calculations and calibration. In *Lecture Notes in Quantum Chemistry*; Roos, B., Ed.; Springer-Verlag: Berlin, 1992; Vol. 58.
- Roothaan, C. C. J. *Rev. Mod. Phys.* **1951**, *23*, 69–89.
- Baldrige, K. K.; Greenberg, J. P. *J. Mol. Graph.* **1995**, *13*, 63.
- Baldrige, K. K.; Schmidt, M. W. *3D-PLTORB*, K1 ed.; San Diego, 1997.
- Baldrige, K. K.; Pederson, L. *Pi Mu Epsilon J.* **1993**, *9*, 513.
- Fukui, K. *The World of Quantum Chemistry*; Reidel: Dordrecht, The Netherlands, 1974.
- Gonzalez, C.; Schlegel, H. B. *J. Phys. Chem.* **1990**, *94*, 5523–5527.
- Schmidt, M. W.; Gordon, M. S.; Dupuis, M. *J. Am. Chem. Soc.* **1985**, *107*, 2585.
- Baldrige, K. K.; Gordon, M. S.; Steckler, R.; Truhlar, D. G. *J. Phys. Chem.* **1989**, *93*, 5107–5119.
- Hehre, W. J.; Radom, L.; Schleyer, P. v. R.; Pople, J. A. *Ab Initio Molecular Orbital Theory*; John Wiley and Sons: New York, 1986.
- Foresman, J. B.; Head-Gordon, M.; Pople, J. A.; Frisch, M. J. *J. Phys. Chem.* **1992**, *96*, 135.
- Woodward, R. B.; Hoffman, R. *The Conservation of Orbital Symmetry*; Verlag Chemie: Weinheim, 1971.
- Schmidt, M. W.; Gordon, M. S. *Annu. Rev. Phys. Chem.* **1998**, *49*, 233–266.
- Edmiston, C.; Ruedenberg, K. Localized atomic and molecular orbitals III. In *Quantum Theory of atoms, molecules, & Solid State*; Löwdin, P. O., Ed.; Academic Press: New York, London, 1966; p 263.